Journal of Theoretical and Applied Vibration and Acoustics 5(1) 69-84 (2019)

I S A V

Journal of Theoretical and Applied Vibration and Acoustics

journal homepage: http://tava.isav.ir

Galloping and VIV control of square-section cylinder utilizing direct opposing smart control force

Amir Hossein Rabiee *

School of Mechanical Engineering, Arak University of Technology, Arak, Iran

ARTICLE INFO

Article history:
Received 20 April 2019

Received in revised form
18 May 2019

Accepted 22 June 2019

Available online 1 July 2019

Keywords:
Galloping,

Flow-induced vibration,

Square-section cylinder,

Intelligent controller,

Active controller.

ABSTRACT

An adaptive fuzzy sliding mode controller (AFSMC) is adopted to reduce the 2D flow-induced vibration of an elastically supported square-section cylinder, free to oscillate in stream-wise and transverse directions in both lock-in and galloping regions. The AFSMC strategy consists of a fuzzy logic inference system intended to follow a sliding-mode controller (SMC), and a robust control system designed to retrieve the variance between the sliding mode and fuzzy controllers. The sprung square cylinder first experiences vortex-induced vibrations with increasing Reynolds number, and then, after passing the critical flow velocity, it confronts high-amplitude and low-frequency vibrations of galloping owning to its sharp corners. A co-simulation platform is considered by linking the AFSMC system modeled in Matlab/Simulink to the plant model implemented in Fluent, aiming at the calculation of opposite control force needed for comprehensive annihilation of the cylinder motions. Based on the performed numerical simulations, it becomes clear that the utilized active control system has successfully mitigated the two-degree-of-freedom vibrations of a square cylinder in both the lock-in region and galloping zone. Here, the vibration amplitudes in the transverse and streamwise directions have decreased by 93% and 94%, for the lock-in region and 93% and 99%, for the galloping zone, respectively.

1. Introduction

Fluid-solid interaction (FSI) is a stimulating engineering subject owing to its numerous applications ranging from pipelines used in different locations to various sections of power plants and heat exchangers[1, 2]. Two interesting phenomena categorized as flow-induced vibration (FIV) are vortex-induced vibration (VIV) and galloping. The former occurs due to the frequency synchronization of vortex-shedding frequency and structural natural frequency, leading to self-excited oscillations with potentially large amplitudes [3]. The latter, i.e. galloping,

* Corresponding author.
E-mail address: rabiee@arakut.ac.ir (A.H. Rabiee)
http://dx.doi.org/10.22064/tava.2019.113251.1144

happens in non-circular cylinders when self-excited instabilities bring about oscillations with different amplitudes[4]. This phenomenon occurs in certain ranges of Reynolds (Re) number that are known to be higher than those of VIV. The cross-flow motion of a structure located in the galloping region yields aerodynamic loads that can augment oscillations [5]. When the flow velocity surpasses a critical galloping velocity, the magnitude of vibrations continues to rise with growing flow velocity. In other words, the criterion that shows the galloping phenomenon takes place is the occurrence of higher amplitude and lower frequency oscillations at higher flow velocities in comparison with lock-in condition for non-circular cylinders. A direct consequence of such vibrations in VIV and galloping is fatigue failure. Accordingly, one must consider different control strategies to alleviate these instabilities [6].

Passive control strategies are best suited for simple applications owing to their easier implementation and independency from an external power source [7]. Obviously, such methods may not be effective in special circumstances as the structural conditions or surrounding properties might change or a modification in the physical characteristics may become obligatory which is usually a challenging task. In contrast, active control methods benefit from actuators that apply energy to desired locations of the system so that the behavioral characteristics of the fluid-structure system could be adjusted[8]. Among such active systems, one can mention rotating cylinders, blowing/suction, acoustic excitation and direct opposing control force [9-12].

Bergers [13] arguably the first researcher who implemented a closed-loop control algorithm to mitigate vortex-shedding of a cylinder at low Re numbers. To reduce VIV in an elastic circular cylinder, Baz and Ro[14] utilized a velocity feedback controller that relied on flow measurements and electromagnetic actuators. A robust adaptive algorithm for a flexible cylinder was developed by Poh and Baz [15] that could effectively control and reduce low-amplitude VIV. The impacts of periodic vortex-induced excitations were greatly eliminated. Such excitations continuously act on flexible cylinders in the same conditions. To control FIV in FSI systems with limited disturbance, Carbonell *et al*.[16] proposed an algorithm with three different approaches. Micro-actuators of PZT type have also been used to empirically mitigate transverse VIV in multiple cylinders as in a study by Li *et al*.[17] In another study, Mehmood *et al*.[18] took advantage of various velocity feedback controllers to actively suppress VIV in a sprung cylinder with a circular cross-section in the synchronization regime. Another study relying on active control methods that sought to mitigate two-dimensional VIV was carried out by Hasheminejad *et al*.[19]. who used the opposite control force on a circular cylinder.

Square cylinders demonstrate a thoroughly distinctive behavior owing to their sharp corners. [20, 21]Venkatraman and Narayanan[22] considered the galloping belonging to a square prism in addition to the vortex-shedding of circular cylinders and proposed an active vibration control approach for these two geometries by modeling them as oscillators with one degree of freedom. A simultaneous control scheme was proposed by Cheng *et al*.[23] to suppress the vibrations in the structure and surrounding flow using a special periodic wave on a piezo actuator. Control systems based on time delay have been the subject of research by Dai *et al*.[24] who evaluated their efficacy in mitigation of large amplitude vibrations of a sprung cylinder of square cross-section. It was shown that the onset of galloping could be delayed using the developed method. Wu *et al*.[25] numerically studied the influence of twist angle on the mitigation of oscillations in a square cylinder that was considered to freely vibrate in the cross-flow direction. It was

demonstrated that the vortex-shedding separation is affected by the twist in the cylinder surface, causing variations in the vortex-shedding frequency and vibration attenuation.

The above introduction shows that despite the large number of studies on the mitigation and control of vibrations due to vortex-shedding in circular cylinders, few studies have dealt with cylinders of square cross-section. Thus, the current study focuses on the topic of an active control strategy on a square cylinder with the aid of application of control forces that has proved to be one of the most appropriate methods for attenuation of FIV in circular cylinders. In this regard, the main novelties of current study are highlighted as follows: (1) Active FIV control of elastically mounted square-section cylinder using direct opposing control force; (2) Simultaneous VIV and galloping control of square-section cylinder; and (3) Application of intelligent model-free control strategy (adaptive fuzzy sliding mode controller) in active FIV control of square cylinder.

2. Formulation

2.1. Mathematical description of fluid and structure

The non-dimensional incompressible Navier-Stokes equations in their two-dimensional form are used to commence the numerical study. They are succinctly described as:

$$\begin{aligned} &\frac{\partial \mathbf{u}}{\partial t} = -(\mathbf{u}.\nabla).\mathbf{u} - \nabla p + \frac{1}{\mathrm{Re}}\nabla^2 \mathbf{u}, \\ &\nabla.\mathbf{u} = 0, \end{aligned} \tag{1}$$

in which p and ρ are the pressure and density of the considered fluid, respectively, and $\mathbf{u}=(u_x/U, u_y/U)$ denotes the non-dimensional velocity vector of flow where U is used to represent the free flow velocity. The oscillating moments and forces are the excitations required for the onset of motion of a rigid body placed in fluid. Here, the two-degree-of-freedom vibration of a rigid sprung cylinder with square cross-section upon which an outer control force via the intelligent control system is exerted is studied. Figure 1 displays a simplified view of the flow around the described cylinder installed on a two-degree-of-freedom elastic base. Along the x direction, the free stream flow causes variable forces, hence the rigid-body motion of the cylinder in both streamwise and transverse direction. An appropriate method for modeling the elastic cylinder is the simplified system of mass-damper-spring with stiffness values of $k_x=k_y=k$, and damping values of $c_x = c_y = c$. The corresponding motion equations are explained as:

$$\begin{aligned} \ddot{x} &= (F_{\mathrm{D}} - c\dot{x} - kx)/m, \\ \ddot{y} &= (F_{\mathrm{L}} - c\dot{y} - ky + F_{\mathrm{a}})/m, \end{aligned} \tag{2}$$

where m is the system mass per unit length, F_{D} and F_{L} are, respectively, the streamwise and transverse forces exerted on the cylinder from the flow and F_{a} is the transverse control force from the actuator (refer to Figure 1). Besides, $\ddot{x}$ and $\ddot{y}$ are, respectively, the in-line and cross-flow accelerations, $\dot{x}$ and $\dot{y}$ are, respectively, the in-line and cross-flow velocities, and x and y are the in-line and cross-flow displacements of the cylinder.

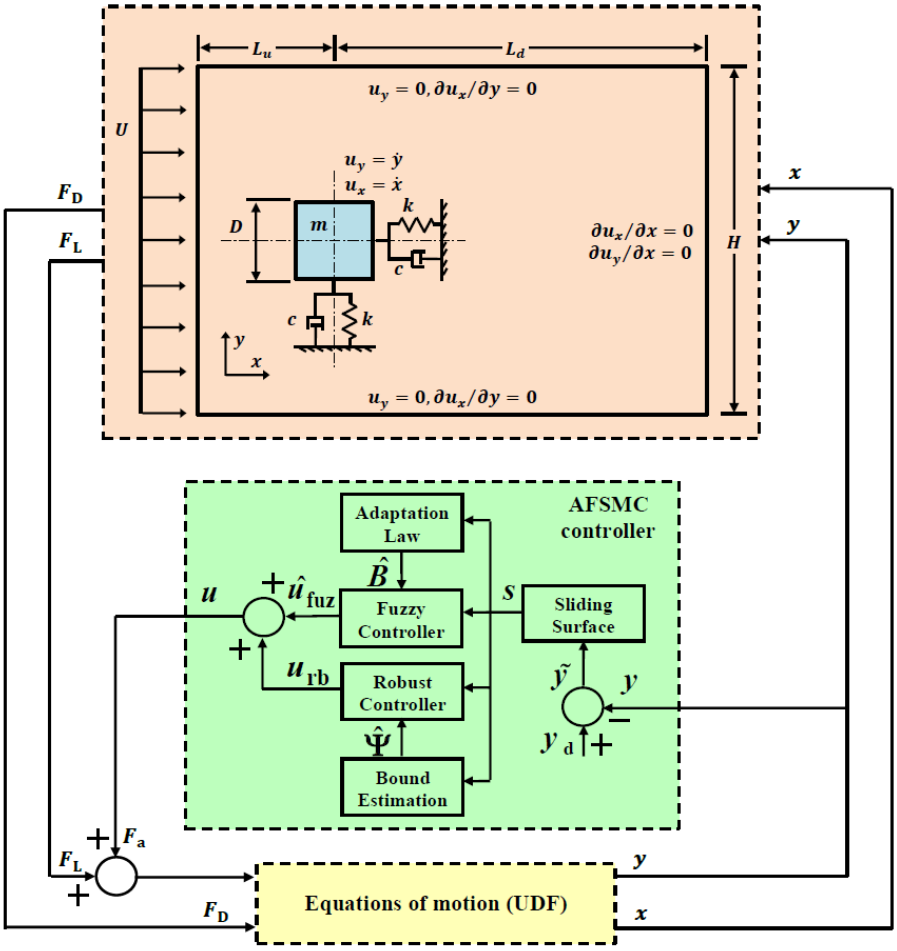

Fig. 1. Representation of FIV on a cylinder with square cross-section along with the adaptive fuzzy sliding mode control block diagram

2.2. Fluid and oscillator solvers

In this section, a summary of the utilized solvers for fluid and structure and their associated properties are discussed. To this aim, ANSYS Fluent combined with a user-defined function (UDF) is used to solve Equation (1) aided by an iteration method. The surrounding domain of the cylinder is a simple rectangle. As displayed in Figure 1, (L_u, L_d) denotes the distances from the center of the cylinder to the boundaries of the upstream and downstream flows, H represents the size of the sidewise boundary and $B = D/H$ is the blockage ratio. The obtained mesh for $B = 0.05$ is shown in Figure 2. A mesh deformation function controls how the triangular grids are shaped after each time step. At the same time, the cylinder is rotated inside the domain and vibration-related quantities are obtained. In addition, unstructured meshes need to be reformed in the outer region. Laminar unsteady properties are taken for the flow in question. Also, hydrodynamic forces are obtained based on a first-order implicit solver using continuity and momentum equations. According to these hydrodynamic forces, the UDF can determine the motion of the elastically-supported square cylinder in terms of velocities in two directions. A

condition for the surface boundary, i.e. $(\dot{x}_{n+1}, \dot{y}_{n+1}) = (u_x, u_y)$, yields results concerning cylinder position, mesh structure and surface flow velocity in an iterative manner. Other assumptions including non-slip boundary conditions on the surface of cylinder, zero stress on horizontal boundaries and zero transverse velocity are important. Refs.[11, 26] provides a more detailed explanation of the flow-structure interaction procedure.

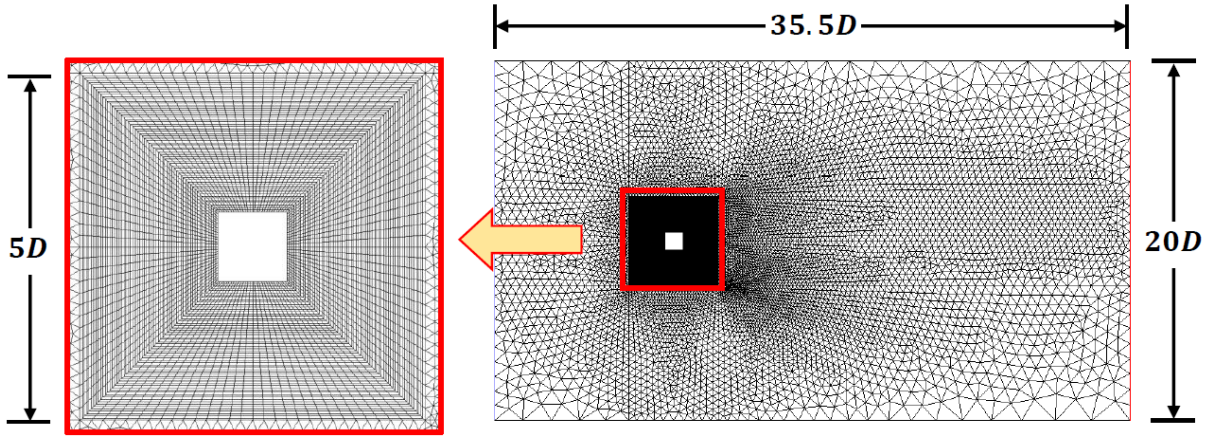

Fig. 2. Schematic of the computational domain

2.3. Controller design

The control of the cylinder understudy constitutes a complex FIV problem whose accurate model is significantly challenging to obtain due to nonlinearities, uncertainties, and variable parameters. This makes the derivation of controller design a cumbersome and even impractical task. Obviously, common control strategies that rely on the mathematical model of plants including sliding mode control (SMC) and $\mathcal{H}2$ / $\mathcal{H}\infty$ robust control are not applicable here. A proper solution to tackle this issue is to use model-free or intelligent control methods based on heuristic algorithms**.**

The adaptive fuzzy sliding mode control (AFSMC) is based on fuzzy concepts and is an appropriate choice for the investigated problem. This method has also been used in various industrial areas [27, 28]. When designing the adaptive fuzzy sliding mode controller, one should consider the interaction between structure and fluid as the controller employs a transverse force F_a to modify this interaction. At its heart, a fuzzy logic control (FLC) algorithm simulates a perfect sliding mode controller, accompanied by a robust controller able to compensate the differences between the fuzzy system and the perfect controller via an adaptive tuning technique targeting FLC parameters and uncertainty bounds related to robust controller[29, 30].

To begin, a condensed inspection of the simple SMC as a method offering concurrent robustness and stability especially in nonlinear control systems is a must. To this end, an affine form of the coupled motion equations previously presented in Equation (2) is required as in:

$$\ddot{y} = f(\mathbf{x}) + g(\mathbf{x})u, \tag{3}$$

where the functions $f(\mathbf{x})$ and $g(\mathbf{x})$ are unknown at this stage, the control input is described by $u=[F_{\mathrm{a}}]$ and the states are hidden in $\mathbf{x}$ as $\mathbf{x}=[x,\dot{x},y,\dot{y}]^T$ with T denoting the vector transpose. Moreover, according to Figure 1, the tracking error is expressed as $\tilde{y}(t)=y_{\mathrm{d}}(t)-y(t)$ where $y_{\mathrm{d}}(t)$ is the preferred state trajectory while the final objective is $\lim_{t\to\infty}\tilde{y}(t)=0$. In the presence of uncertainties, a description of the previous second-order system is best written as:

$$\ddot{y}=f(\mathbf{x})+g(\mathbf{x})u+d, \tag{4}$$

in which $|d|\le\delta$ ($d=\Delta f(\mathbf{x})+\Delta g(\mathbf{x})u$) signifies the bounded uncertainty parameter. Next, a description of the sliding surface ,as well as its derivate, should be given in the form:

$$\begin{aligned} s&=\dot{\tilde{y}}+\lambda\tilde{y},\\ \dot{s}&=\ddot{y}_{\mathrm{d}}-\ddot{y}+\lambda\dot{\tilde{y}}, \end{aligned} \tag{5}$$

where λ is not known at this stage. Finally, SMC rule is described as:

$$u=u_{\mathrm{eq}}+u_{\mathrm{rb}}, \tag{6}$$

where u_{eq} is the equivalent feedback controller defined as $u_{\mathrm{eq}}=g^{-1}(\mathbf{x})\left[-f(\mathbf{x})+\ddot{y}_{\mathrm{d}}+\lambda\dot{\tilde{y}}\right]$ and found through the use of Equation (3) and Equation (5) assuming $\dot{s}=0$. Also, u_{rb} defined as $u_{\mathrm{rb}}=g^{-1}\left[\delta\,\mathrm{sgn}(s)\right]$ is necessary to be able to consider uncertainties.

Next, minimization of uncertainty bounds to eliminate chattering and to attain closed-loop stability is necessary. One should note that the ideal input for the controller, Equation (6), is not achievable as the required parameters are not known beforehand. To tackle this issue, u_{eq} is estimated using an ideal controller u^* based on the concept of a Takagi-Saugeno fuzzy system having a single input (shown by *s*), a single output (shown by u_{fuz}) and n_r fuzzy IF-THEN rules:

Rule *r* : IF s is A^r THEN $\quad u_{\mathrm{fuz}}=b^r,\quad (r=1,\ldots,n_r),$ (7)

where A^r is a fuzzy set based on a special membership function described by $\mu_{A^r}(s)=e^{-[(s-c^r)/\sigma^r]^2}$ in which c^r and σ^r are the corresponding center and width, and b^r signifies a fuzzy singleton related to the output value of the *r*-th rule. Now, the fuzzy system output based on a well-known fuzzy interference method is expressed as:

$$u_{\mathrm{fuz}}(s,\mathbf{B})=\mathbf{B}^{\mathrm{T}}\mathbf{W}, \tag{8}$$

where $\mathbf{B}=[b^1,\ldots,b^{n_r}]^{\mathrm{T}}$ and $\mathbf{W}=[w^1,\ldots,w^{n_r}]^{\mathrm{T}}$ with $w^r=\mu_{A^r}(s)\left[\sum_{r=1}^{n_r}\mu_{A^r}(s)\right]^{-1}$ indicating the firing strength of the previous section of a fuzzy rule.

It is now time to approximate the u^* using an ideal fuzzy controller in the form:

$$u^* = u^*_{\text{fuz}}(s, \mathbf{B}^*) + \psi = \mathbf{B}^{*\text{T}}\mathbf{W} + \psi, \tag{9}$$

where $\mathbf{B}^*$ is the optimal parameter vector defined by $\mathbf{B}^* \triangleq \arg\min_{\mathbf{B}} \left\{ \left| \mathbf{B}^T\mathbf{W} - u^* \right| \right\}$ and ψ is the sum of errors due to imperfect approximation and any other uncertainty ($|\psi| < \Psi$). Generally, $\mathbf{B}^*$ and Ψ are not exactly known, hence the need for an estimation. Also, $\hat{u}_{\text{fuz}}$ as a means of estimating the ideal controller is expressed as:

$$\hat{u}_{\text{fuz}}(s, \hat{\mathbf{B}}) = \hat{\mathbf{B}}^{\text{T}}\mathbf{W}, \tag{10}$$

quantity $\hat{\mathbf{B}}$ is an estimation of $\mathbf{B}^*$. At this point, one can propose a proper control law for the AFSMC system as in:

$$u = \hat{u}_{\text{fuz}}(s, \hat{\mathbf{B}}) + u_{\text{rb}}(s), \tag{11}$$

where u_{rb} takes care of the discrepancies between ideal and fuzzy controllers. Substituting Equation (15) in Equation (7) results in:

$$\ddot{y} = f(\mathbf{x}) + g(\mathbf{x})[\hat{u}_{\text{fuz}}(s, \hat{\mathbf{B}}) + u_{\text{rb}}(s)]. \tag{12}$$

Additionally, by considering a set of approximation errors in the form $\tilde{u}_{\text{fuz}} = u^* - \hat{u}_{\text{fuz}}$, $\tilde{\mathbf{B}} = \mathbf{B}^* - \hat{\mathbf{B}}$, and $\tilde{\Psi} = \Psi - \hat{\Psi}$ in which $\hat{\Psi}$ is an estimation of uncertainty bound, and with the aid of Equations (9) and (10), one arrives at:

$$\tilde{u}_{\text{fuz}} = \tilde{\mathbf{B}}^{\text{T}}\mathbf{W} + \psi, \tag{13}$$

It should be restated that $|\psi| < \Psi$.

The proposed design steps of AFSMC are listed as:

a) Choosing a control input according to Equation (11)

b) Adaptively tuning the fuzzy parameter vector as explained by:

$$\dot{\hat{\mathbf{B}}} = -\dot{\tilde{\mathbf{B}}} = \alpha_1 s(t)\mathbf{W}, \tag{14}$$

c) Determining a robust controller according to:

$$u_{\text{rb}} = \hat{\Psi}\,\text{sgn}[s(t)]\text{sgn}[g(t)], \tag{15}$$

d) Approximating the uncertainty bound in an adaptive manner as in:

$$\dot{\hat{\Psi}} = -\dot{\tilde{\Psi}} = \alpha_2 |s(t)|\text{sgn}[g(t)], \tag{16}$$

Where α_1 and α_2 are the learning rates assigned by the user, and it is desired that $\lim_{t\to\infty} \tilde{y}(t) = 0$.

2.4. Fluent/Matlab Coupling, grid independency study, and validation

ANSYS Fluent and MATLAB/Simulink are used to implement the CFD and control models, respectively. An appropriate coupling and a concurrent simulation scheme are proposed between the two as in Figure 1 such that the controller recalls the outputs of the CFD model and attempts to control the cylinder vibrations. In particular, the communications of utilized data between Matlab/Simulink and ANSYS/Fluent are attained through a simple test file. The detailed procedure is as follows: (1) The ANSYS/Fluent solver calculates the pressure and velocity in the computational domain, (2) Fluid forces in the streamwise and transverse ($F_{\mathrm{D}}, F_{\mathrm{L}}$) directions are found, (3) The total force on the cylinder is obtained using the UDF, (4) The solution of motion equations is found using the Euler formula in the explicit form, (5) MATLAB reads the computed transverse displacements log, (6) The necessary force for displacement attenuation is found and saved by AFSMC, (7) The UDF reads the required control force as saved in a separate file from the last step, (8) Motion equations are solved once more according to the recalculated total force, (9) The procedure is repeated until the cross-flow displacements of cylinder are entirely eliminated.

It is essential to obtain the appropriate mesh size for precise flow computations. For this purpose, to examine the grid size independency, the general mesh arrangement is maintained, and consequently, the effect of the relative grid enhancement on the calculated mean drag and maximum lift coefficients associated with stationary square-section cylinder at Re=100 is investigated. Three different mesh grids of different sizes have been explored, as listed in Table 1, in which the level of improvement of the grids increasing for each case. According to computed force coefficients presented in Table 1, one can see the convergence of the calculated solution on gradually smaller mesh grids. Subsequently, the second grid (Case 2) with medium mesh grid quality appears to be the finest candidate intended for employment in the collaborative simulations hereafter. This selection approves that perfect compromise will be obtained between numerical precision and computing effort.

Table1. Effect of mesh grid improvement on the computed force coefficients of the elastically-mounted square-section cylinder

	Total no. of cells	No. of cells in the central block	$C_{\mathrm{L}}^{\max}$	$\bar{C}_{\mathrm{D}}$
Case 1	9100	3000	0.382	**1.662**
Case 2	20000	7000	0.339	1.607
Case 3	64500	9500	0.333	1.601

As an important step, the conducted simulations should be validated so as to check the reliability of the proposed method. The value of necessary quantities is taken as $m^{*}=10, \xi=0, B=0.05; F_N = f_N D/U = 14.39/\mathrm{Re}$ based on which the variations in the maximum amplitude of the cross-flow vibration of a flexibly supported square cylinder with two degrees of freedom at various Re numbers and a constant blockage ratio (B = 0.05) are obtained. The results closely match the findings of Sen and Mittal [31] who employed a finite element code (see Figure 3a).

3. Numerical results

To study how VIV and galloping respond to the adaptive fuzzy sliding mode controller, the same parameters used in the previous section are employed.[31] Figure 2 displays the domain assuming $H = 20D$ and B = 0.05 for CFD analysis. The total number of grid cells reaches 20000 while those in the center grid count up to 7000. For the lock-in and galloping zones, Re numbers of $\mathrm{Re} = 87.5$ and $\mathrm{Re} = 250$ are considered, respectively. As discussed earlier, we seek to completely eliminate the cylinder vibration in the cross-flow direction, i.e. $y_{\mathrm{d}}(t) = 0$ while AFSMC attempts to satisfy the relation $\lim_{t\to\infty} \tilde{y}(t) = 0$. Other required parameters are taken as $\lambda = 3$, $(c^r, \sigma^r) = (-10,3),(0,3),(10,3)$, $\hat{B} = [-0.5,0,0.5]$ and $\Psi = 0.1$. Moreover, the learning rates are set to α_1 =0.02 and α_2 =0.025.

Practical implementation concerns, including sensors, actuators ,and installation considerations, are not included in the main scope of the present study. However, a brief and simple explanation of the practical set up for considered FIV closed-loop control system is provided. The opposing control force should be attained by the utilization of electromagnetic actuator mounted inside the cylinder, to prevent flow distribution around the cylinder [14, 32]. The feedback signal (cylinder transverse displacement) can be achieved utilizing either a direct displacement sensor (laser displacement senor or LVDT) or a small accelerometer sensor mounted inside the surface of the square cylinder. To calculate cylinder position information, the accelerometer data can be integrated two times, and the output sent to the control system. Next, the control signal should be amplified and then drive the utilized actuator.

For both uncontrolled and control configurations, Figure 3b displays the outputs of the time evolution response related to the dimensionless displacements in the transverse and streamwise directions corresponding to Re numbers of lock-in and galloping zones, i.e. $\mathrm{Re} = 87.5$ and $\mathrm{Re} = 250$, respectively. First, for the lock-in region, the oscillation frequency of transverse displacement turns out to be almost the same as the vortex-shedding frequency. The corresponding frequency of streamwise displacement is, however, twice as much. According to the conducted analysis, the vibration amplitudes in the transverse and streamwise directions have decreased by 93% and 94%, respectively, thanks to the performance of the adaptive fuzzy sliding mode controller. On the other hand, for the galloping zone, the proposed controller has decreased the transverse and streamwise oscillations by as much as 93% and 99%, respectively. Compared with the lock-in region, the uncontrolled response of the square cylinder has considerably increased in the galloping zone. This is especially true about the streamwise vibrations. As observed, although the control force is only exerted in the transverse direction to the cylinder, its vibration is also significantly reduced in the streamwise direction. This is due to the coupling between motion equations in the *x* and *y* direction of the flow-dependent cylinder. The decrease in the cylinder transverse vibration alters the fluid-structure nature around the cylinder, resulting in the reduction of its streamwise vibration.

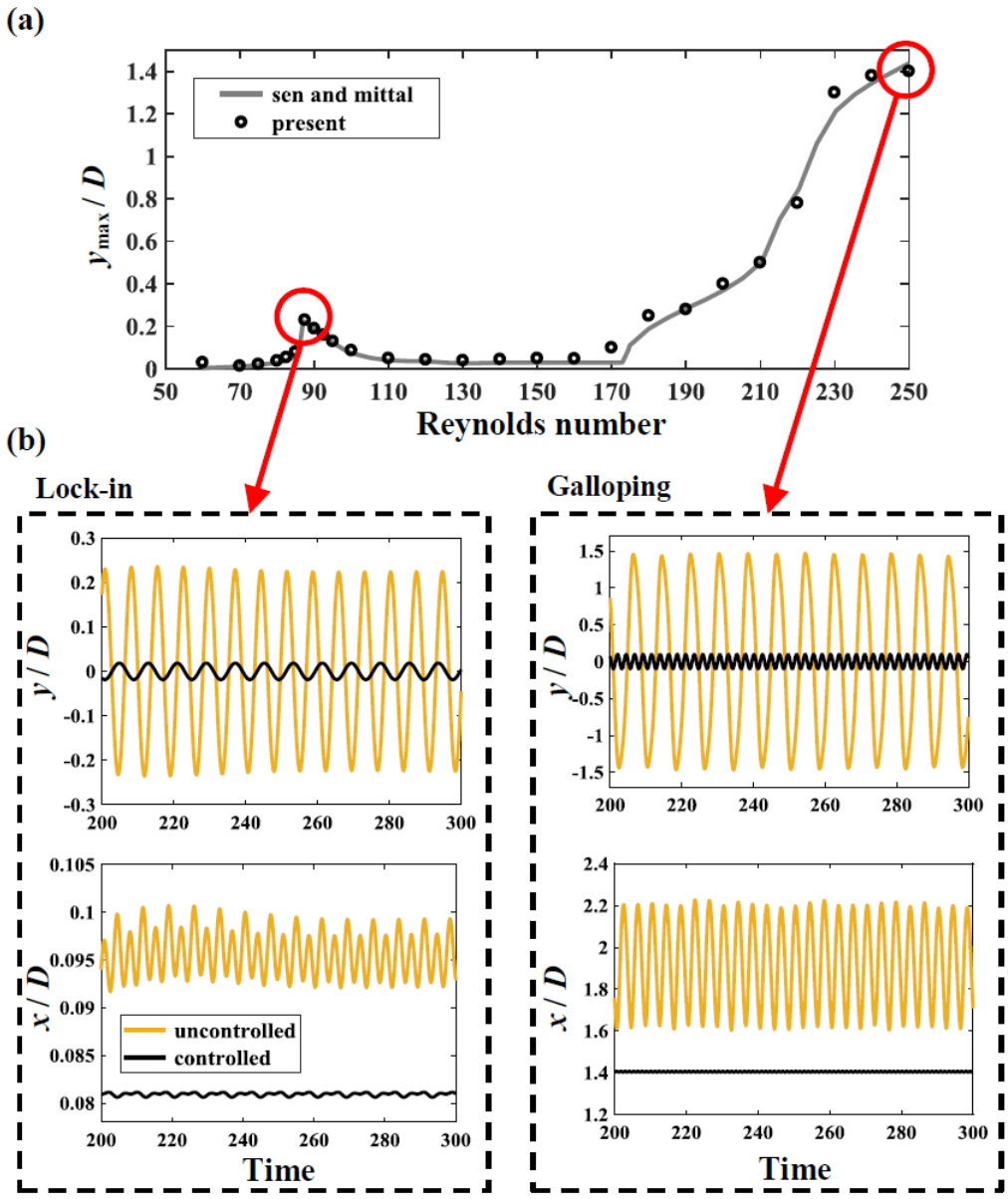

Fig. 3. (a) Representation of changes in the amplitude of cross-flow displacement at different Re numbers, (b) Outputs of the time evolution response related to the dimensionless displacements in the transverse and streamwise directions in both lock-in and galloping regions.

For both controlled and uncontrolled cases, the orbital trajectories, i.e. y/D vs x/D, of the sprung cylinder understudy at $\mathrm{Re}=87.5$ (lock-in region) and $\mathrm{Re}=250$ (galloping zone) are shown in Figure 4. The 8-shaped traces offer a proper view of oscillations in both streamwise and transverse directions after a cycle. For a better representation of the described condition, the magnified view of the orbital trajectory of the cylinder in the controlled case is presented on its right side. The adaptive fuzzy sliding mode controller has thoroughly miniaturized the orbital traces in addition to shifting them to the left side such that the displacement magnitude in both

directions has successfully approached zero. This was also identifiable in the black plots of the figure.

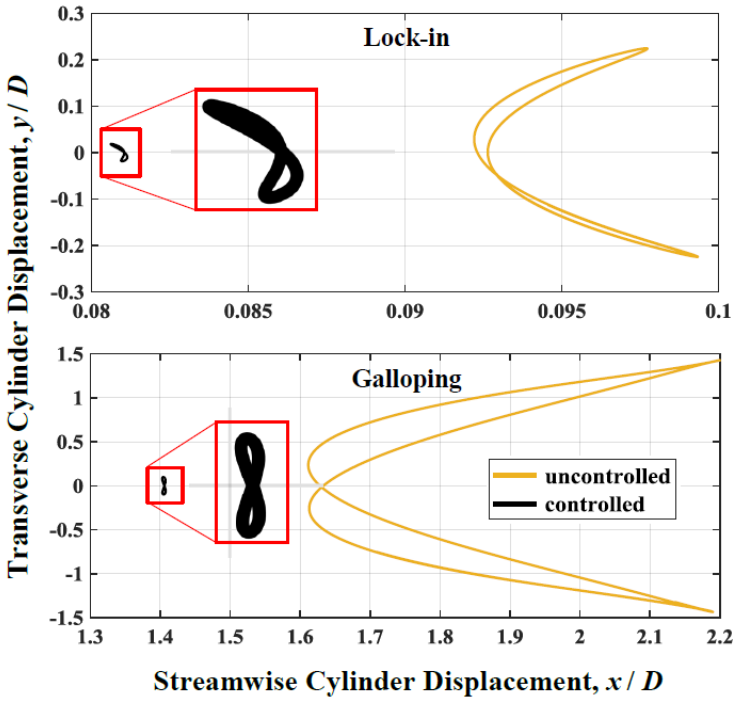

Fig. 4. Orbital trajectories of square-section cylinder for controlled and uncontrolled cases in both lock-in and galloping regions

For both controlled and uncontrolled cases, the values of lift and drag coefficients in both studied regions are provided in the form of time evolution responses as in Figure 5. The amplitude of the lift coefficient on the cylinder in the lock-in region shows no reduction compared with the uncontrolled case. Also, the frequency change in the lift coefficient is clearly visible. On the contrary, the active controller has successfully decreased the magnitude of drag coefficient on the cylinder by 97%. At $\mathrm{Re} = 250$ (galloping zone), the adaptive fuzzy sliding mode controller has decreased the amplitudes of drag and lift coefficients by 90% and 50%, respectively. The obtained results show that the active control system has not performed satisfactorily in reducing the amplitude of lift coefficient on the cylinder, particularly in the lock-in region. In contrast, the transverse displacement amplitude of cylinder for both studied regions has reduced by more than 90%. This indicates that the main reason behind the reduction in the cylinder transverse vibration is not the decrease in the magnitude of lift coefficient.

For both galloping and lock-in regions, the values of power spectral density (PSD) related to both controlled and uncontrolled cases can be seen in Figure 6 as a means of better assessment. The normalized values of vortex-shedding frequency in the lock-in region ($f/f_n = 1$) related to the uncontrolled cylinder show they are almost equal to the structural natural frequency, indicating the resonance in the structure. Another advantage of the control system is demonstrated by the reduction of normalized vortex-shedding frequency to $f/f_n = 0.84$ (from a previous value of $f/f_n = 1$). As a result, the transferred energy from the fluid flow to the square

cylinder has considerably decreased after the interruption in frequency synchronization. A direct consequence of this phenomenon is a 93% decrease in the amplitude of transverse vibrations. Furthermore, the normalized vortex-shedding frequency in the galloping region, i.e. $f/f_n = 0.87$, has shifted up to $f/f_n = 2.92$ using the active controller. Consequently, the galloping oscillation frequency, which occurs in lower values than lock-in frequency, has risen and thus, the square cylinder exits this region due to the frequency change.

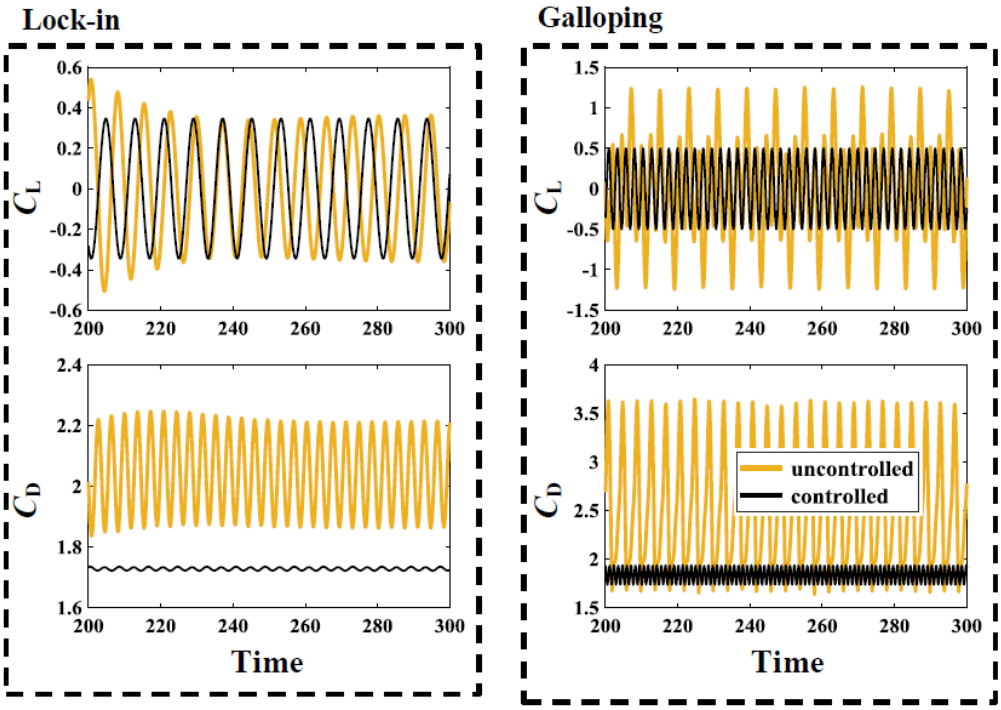

Fig. 5. Lift and drag coefficients in the form of time evolution responses for controlled and uncontrolled cases in both lock-in and galloping regions

The snapshots of steady-state vorticity patterns corresponding to adaptive fuzzy sliding mode controlled and uncontrolled cylinder at $\mathrm{Re} = 87.5$ and $\mathrm{Re} = 250$ are provided in Figure 7. The associated snapshot for the stationary cylinder can also be seen to compare different cases. In the lock-in region, the wake vorticity pattern toward the back of the uncontrolled circular cylinder demonstrates the 2S mode. In this condition, a single vortex from the top and bottom boundaries of the cylinder is reciprocally shed after a vibration cycle. Here, with the aim of an active control system, no change in the mode of vorticity has been made while the vortex sizes have been slightly reduced and the distance between them has increased. On the other hand, in the galloping region, the 2P mode can be seen in the vorticities. This occurs when a pair of vortices (double-vortex) from the top and bottom boundaries are reciprocally shed from the cylindrical structure after a vibration cycle. Here, the adaptive fuzzy sliding mode controller successfully shifts the 2P mode vortices to the regular 2S-mode of von Kármán vortex shedding. Also, the size and the distance between the vortexes are reduced compared with the uncontrolled case. Finally, it is observed that by employing an active control system, the general shape of vortexes

formed toward the back of the square cylinder is similar to a stationary square cylinder, indicating the small amplitude of cylinder oscillations.

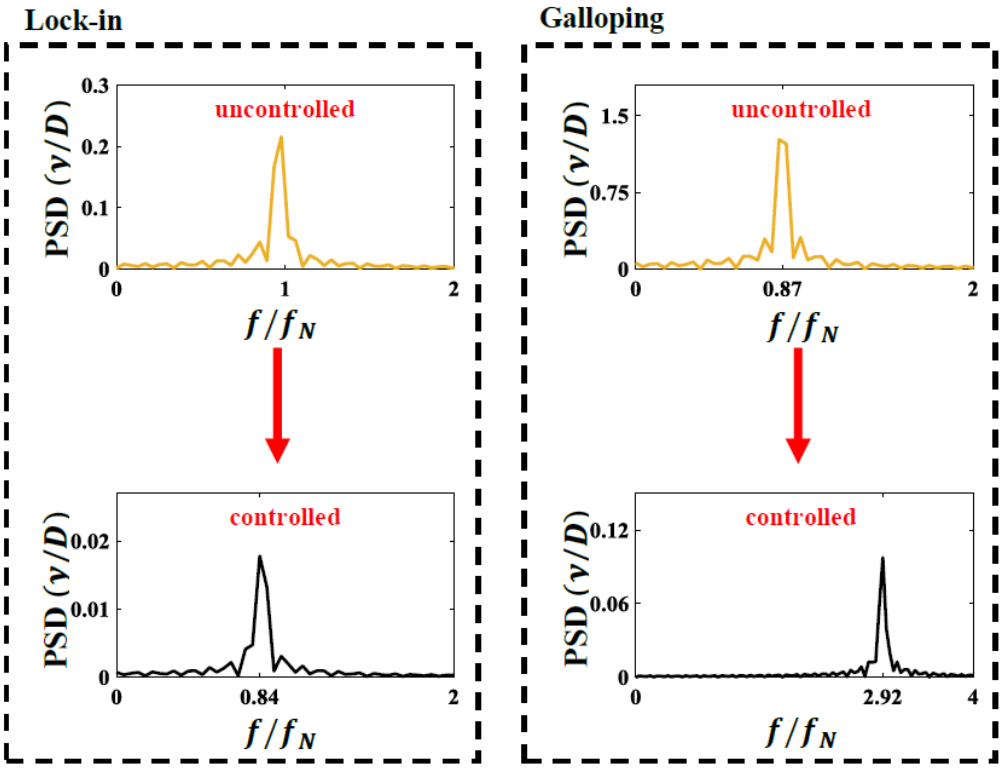

Fig. 6. PSD of cylinder transverse displacement for both controlled and uncontrolled cases

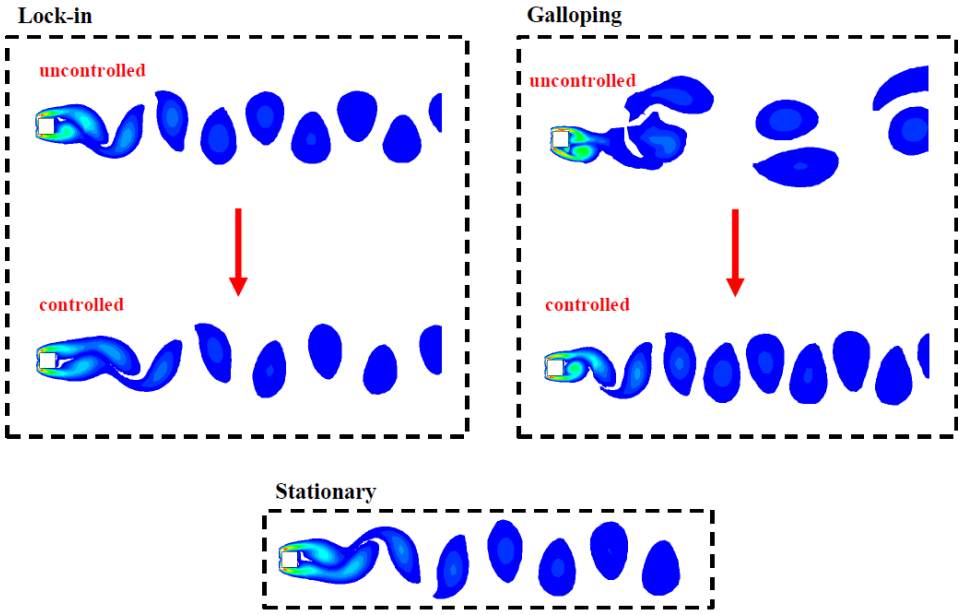

Fig. 7. Snapshots of instantaneous vorticities for both lock-in and galloping regions

4. Conclusions

An adaptive fuzzy sliding mode control strategy is employed to annihilate the two-dimensional vortex-induced vibration and galloping of a sprung square-section cylinder at Reynolds numbers of $\mathrm{Re}=87.5$ and $\mathrm{Re}=250$. A co-simulation platform is considered by linking the AFSMC system modeled in Matlab/Simulink to the plant model implemented in Fluent, aiming at calculation of opposite control force needed for comprehensive suppuration of the cylinder motions. The most important observations are as follows. The sprung square cylinder first experiences vortex-induced vibrations with increasing Reynolds number, and then, after passing the critical flow velocity, it confronts high-amplitude and low-frequency vibrations of galloping owning to its sharp corners. First, for the lock-in region, the vibration amplitudes in the transverse and streamwise directions have decreased by 93% and 94%, respectively by utilization of an active control system. Moreover, for the galloping zone, the proposed controller has decreased the transverse and streamwise oscillations by as much as 93% and 99%, respectively. Also, the amplitude of the lift coefficient on the cylinder in the lock-in region shows no reduction compared with the uncontrolled case. At the galloping zone, the adaptive fuzzy sliding mode controller has decreased the amplitudes of lift coefficients only by 50%. The obtained results show that the active control system has not performed satisfactorily in reducing the amplitude of lift coefficient on the cylinder, particularly in the lock-in region. This indicates that the main reason behind the reduction in the cylinder transverse vibration is not the decrease in the magnitude of lift coefficient. On closer examination, it can be seen that the utilized controller reduces the normalized vortex-shedding frequency from $f/f_n=1$ to $f/f_n=0.84$. As a result, the transferred energy from the fluid flow to the square cylinder has considerably decreased after the interruption in frequency synchronization. Furthermore, the normalized vortex-shedding frequency in the galloping region, i.e. $f/f_n=0.87$, has shifted up to $f/f_n=2.92$ using the active controller. Consequently, the galloping oscillation frequency, which occurs in lower values than lock-in frequency, has risen and thus, the square cylinder exits this region due to the frequency change. Finally, it is observed that by employing an active control system, the general shape of vortices formed toward the back of the square cylinder is similar to a stationary square cylinder, indicating the small amplitude of cylinder oscillations.

References

[1] M. Keber, M. Wiercigroch, Dynamics of a vertical riser with weak structural nonlinearity excited by wakes, Journal of Sound and Vibration, 315 (2008) 685-699.
[2] V.D. Tandel, R.V. Patil, A Survey on vortex induced vibration of cross flow heat exchanger tubes, International Journal of Engineering Research and Technology, 3 (2014).
[3] N.A. Capell, D.W. Carlson, Y. Modarres-Sadeghi, Vortex-induced vibration of a single degree-of-freedom flexibly-mounted horizontal cylinder near the free surface, Journal of Sound and Vibration, 444 (2019) 161-175.
[4] H. Jayatunga, B.T. Tan, J. Leontini, A study on the energy transfer of a square prism under fluid-elastic galloping, Journal of Fluids and Structures, 55 (2015) 384-397.
[5] S. Sen, S. Mittal, Free vibration of a square cylinder at low Reynolds numbers, Journal of Fluids and Structures, 27 (2011) 875-884.
[6] S.M. Hasheminejad, A.H. Rabiee, H. Bahrami, Active closed-loop vortex-induced vibration control of an elastically mounted circular cylinder at low Reynolds number using feedback rotary oscillations, Acta Mechanica, 229 (2018) 231-250.
[7] R.A. Kumar, C.-H. Sohn, B.H. Gowda, Passive control of vortex-induced vibrations: an overview, Recent Patents on Mechanical Engineering, 1 (2008) 1-11.

[8] A.H. Rabiee, Regenerative semi-active vortex-induced vibration control of elastic circular cylinder considering the effects of capacitance value and control parameters, Journal of Mechanical Science and Technology, 32 (2018) 5583-5595.
[9] N. Fujisawa, G. Takeda, N. Ike, Phase-averaged characteristics of flow around a circular cylinder under acoustic excitation control, Journal of Fluids and Structures, 19 (2004) 159-170.
[10] W.-L. Chen, D.-B. Xin, F. Xu, H. Li, J.-P. Ou, H. Hu, Suppression of vortex-induced vibration of a circular cylinder using suction-based flow control, Journal of Fluids and Structures, 42 (2013) 25-39.
[11] S.M. Hasheminejad, A.H. Rabiee, M. Jarrahi, A. Markazi, Active vortex-induced vibration control of a circular cylinder at low Reynolds numbers using an adaptive fuzzy sliding mode controller, Journal of Fluids and Structures, 50 (2014) 49-65.
[12] J. Jiménez-González, F. Huera-Huarte, Vortex-induced vibrations of a circular cylinder with a pair of control rods of varying size, Journal of Sound and Vibration, 431 (2018) 163-176.
[13] E. Berger, Suppression of vortex shedding and turbulence behind oscillating cylinders, The Physics of Fluids, 10 (1967) 191-193.
[14] A. Baz, J. Ro, Active control of flow-induced vibrations of a flexible cylinder using direct velocity feedback, Journal of Sound and Vibration, 146 (1991) 33-45.
[15] S. Poh, A. Baz, A demonstration of adaptive least-mean-square control of small amplitude vortex-induced vibrations, Journal of fluids and structures, 10 (1996) 615-632.
[16] P. Carbonell, X. Wang, Z.P. Jiang, On the suppression of flow-induced vibration with a simple control algorithm, Communications in Nonlinear Science and Numerical Simulation, 8 (2003) 49-64.
[17] B.-Q. Li, Y. Liu, J.-R. Chu, Vortex-induced vibration control by micro actuator, Journal of mechanical science and technology, 21 (2007) 1408.
[18] A. Mehmood, A. Abdelkefi, I. Akhtar, A.H. Nayfeh, A. Nuhait, M.R. Hajj, Linear and nonlinear active feedback controls for vortex-induced vibrations of circular cylinders, Journal of Vibration and control, 20 (2014) 1137-1147.
[19] S.M. Hasheminejad, A.H. Rabiee, A. Markazi, Dual-Functional Electromagnetic Energy Harvesting and Vortex-Induced Vibration Control of an Elastically Mounted Circular Cylinder, Journal of Engineering Mechanics, 144 (2017) 04017184.
[20] M. Zhao, L. Cheng, T. Zhou, Numerical simulation of vortex-induced vibration of a square cylinder at a low Reynolds number, Physics of Fluids, 25 (2013) 023603.
[21] A.H. Dawi, R.A. Akkermans, Direct and integral noise computation of two square cylinders in tandem arrangement, Journal of Sound and Vibration, 436 (2018) 138-154.
[22] K. Venkatraman, S. Narayanan, Active control of flow-induced vibration, Journal of sound and vibration, 162 (1993) 43-55.
[23] L. Cheng, Y. Zhou, M. Zhang, Controlled vortex-induced vibration on a fix-supported flexible cylinder in cross-flow, Journal of sound and vibration, 292 (2006) 279-299.
[24] H. Dai, A. Abdelkefi, L. Wang, W. Liu, Control of cross-flow-induced vibrations of square cylinders using linear and nonlinear delayed feedbacks, Nonlinear Dynamics, 78 (2014) 907-919.
[25] C.-H. Wu, S. Ma, C.-W. Kang, T.-B. Lim, R.K. Jaiman, G. Weymouth, O. Tutty, Suppression of vortex-induced vibration of a square cylinder via continuous twisting at moderate Reynolds numbers, Journal of Wind Engineering and Industrial Aerodynamics, 177 (2018) 136-154.
[26] S.M. Hasheminejad, A.H. Rabiee, M. Jarrahi, Semi-active vortex induced vibration control of an elastic elliptical cylinder with energy regeneration capability, International Journal of Structural Stability and Dynamics, 17 (2017) 1750107.
[27] A.H. Rabiee, A.H. Markazi, Semi-active adaptive fuzzy sliding mode control of buildings under earthquake excitations, in: Proceedings of the 2nd World Congress on civil, structural, and environmental engineering, Barcelona, Spain, 2017.
[28] G. Susheelkumar, S. Murigendrappa, K. Gangadharan, Theoretical and experimental investigation of model-free adaptive fuzzy sliding mode control for MRE based adaptive tuned vibration absorber, Smart Materials and Structures, 28 (2019) 045017.
[29] A. Poursamad, A.H. Davaie-Markazi, Robust adaptive fuzzy control of unknown chaotic systems, Applied Soft Computing, 9 (2009) 970-976.
[30] H. Navvabi, A.H. Markazi, Hybrid position/force control of Stewart Manipulator using Extended Adaptive Fuzzy Sliding Mode Controller (E-AFSMC), ISA transactions, 88 (2019) 280-295.

[31] S. Sen, S. .Mittal, Effect of mass ratio on free vibrations of a square cylinder at low Reynolds numbers, Journal of Fluids and Structures, 54 (2015) 661-678.
[32] H. Warui, N. Fujisawa, Feedback control of vortex shedding from a circular cylinder by cross-flow cylinder oscillations, Experiments in Fluids, 21 (1996) 49-56.